Molecular Crystals and Liquid Crystals Science and Technology. Section A. Molecular Crystals and Liquid Crystals

Publication details, including instructions for authors and subscription information:
http://www.tandfonline.com/loi/gmcl19

Erratum

Version of record first published: 24 Sep 2006

To cite this article: (2000): Erratum, Molecular Crystals and Liquid Crystals Science and Technology. Section A. Molecular Crystals and Liquid Crystals, 350:1, 297-305

To link to this article: http://dx.doi.org/10.1080/10587250008025252

Mol. Cryst. Liq. Cryst., Vol. 350, pp. 297-305
Reprints available directly from the publisher
Photocopying permitted by license only

Erratum
Self-Supporting Smectic Bubbles*

R. STANNARIUS[a†], C. CRAMER[b] and H. SCHÜRING[a]

[a]Universität Leipzig, Fakultät für Physik und Geowissenschaften Linnéstr. 5, Leipzig, 04103, Germany and [b]University of Delaware, Newark, DE 19716, USA

Self-supporting smectic bubbles consist of highly ordered membranes of nanometer to micrometer thickness. They can reach radii of several centimeters. Analogous to soap bubbles, they can be generated by excerting lateral pressure on a planar freely suspended smectic film. We describe the optical properties of these objects and the determination of the membrane thickness from transmission images. The dynamics of the growth and motion of holes (regions of reduced number of layers) on the bubble surface is briefly discussed.

Keywords: smectic bubbles; optics

INTRODUCTION

Freely suspended smectic films have attracted considerable interest in the past for the study of optic, electric and dynamic properties of ferroelectric and non-ferroelectric smectic phases[1]. When these films are exposed to external pressure from one side, they bend until a balance between pressure difference and surface tension is established[2]. In this way, self-supporting spherical bubbles can be produced[3,4]. These structures are characterized by a unique ratio of film thickness and sphere diameter which may differ by about 6 orders of magnitude. In this work we study bubbles with radii of several millimeters.

The spherical film is stabilized by the molecular smectic layer structure, comparable in some respect to a soap bubble, although the resemblance is superficial. The smectic membranes are (meta)stable, dynamic thickness fluctuations of the film are excluded. The bubbles persist as long as the inner pressure is kept constant. The surface tension alone is responsible for their spherical shape, it relates membrane

* This manuscript originally appeared in MCLC Volume 329 (1999) pp. 423 – 431. The text in both versions is the same. The following reproduction is to clarify the information in the illustrations.

† Corresponding Author.

curvature and inner excess pressure. Prerequisite for a number of unique experiments with these bubbles is the knowledge of their membrane thickness. Its determination from the optical transmission profile is described here.

EXPERIMENTAL SETUP

Figure 1 sketches the experimental setup. The bubbles are enclosed in a thermocontrol box which protects them against ambient air flow and external disturbances. Temperature is controlled with an accuracy of 0.1K. We illuminate the bubbles with parallel monochromatic light. The transmission images are recorded by means of a HAMAMATSU video camera, digitized and processed in a computer. The experiments have been performed with DOBAMBC in the S_A and S_C^* phases if not stated otherwise. All images shown are approximately 1 cm × 1 cm, Fig. 5b is 4 mm × 4 mm.

OPTICS

The optical transmission images provide information on the thickness d of the bubble membrane. In the center of the images, light passes the bubble at normal incidence, and the equations for optical transmission are equivalent to those for planar smectic films[6]. The new feature of the spherical bubbles is that the angle of incidence θ_a of light onto the smectic film varies across the image in a well defined manner (Fig. 2)

$$\theta_a = \arcsin \frac{r}{R} \tag{1}$$

influencing the effective film thickness, effective refractive index, reflection and transmission at the film surfaces. One image of a homogeneous spherical bubble yields optical information equivalent to the angular scan of a planar film. The thickness d can be determined in principle from one single image with monochromatic illumination (wavelength λ). Figures 2, 3 show the geometry and define the quantities used in our calculations. We consider a smectic A bubble with radius R and film thickness d. The S_A phase is uniaxial with the optical axis normal to the film plane. Ordinar and extraordinary refractive indices are n_e, n_o.

For millimeter bubbles we can neglect the film curvature locally and apply the standard equations for transmission of plane parallel plates[5]. The membrane thickness is very small and therefore we disregard lateral dislocations of the light beam after passing the smectic layer. We calculate the intensity separately for

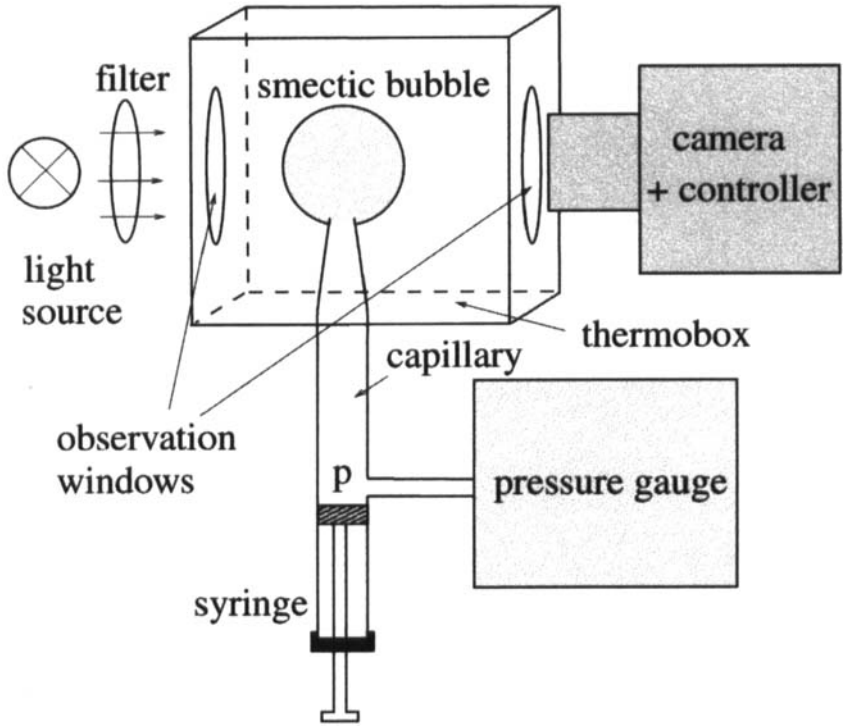

FIGURE 1 Experimental setup for the generation and observation of smectic bubbles. A smectic film prepared on the opening of a glass capillary is inflated to spherical shape. The bubble volume is controlled, the inner excess pressure is measured with a commercial precision gauge. Capillary radii are between 0.5 and 3 mm

each position in the transmission image. The incident light beam can be decomposed into the component polarized in the plane of incidence ((1) and (2) in Fig. 2, index $\|$) and a second component polarized perpendicular to that plane ((3) in Fig. 2, index $\perp$). The latter experiences only the ordinary refractive index. The transmission coefficients for the electric field amplitudes at the air/film and film/air surfaces are

$$\tau_{\perp}^{(in)} = \frac{2\sin\theta_i \cos\theta_a}{\sin(\theta_i + \theta_a)} \text{ and } \tau_{\perp}^{(out)} = \frac{2\cos\theta_i \sin\theta_a}{\sin(\theta_i + \theta_a)} \tag{2}$$

respectively, with $\sin\theta_a = n_o \sin\theta_i$. The internal reflection at the film/air surface is described by the coefficient

$$\rho_{\perp} = \frac{\sin(\theta_a - \theta_i)}{\sin(\theta_a + \theta_i)} \text{ with } \tau_{\perp}^{(in)}\tau_{\perp}^{(out)} = 1 - \rho_{\perp}^2. \tag{3}$$

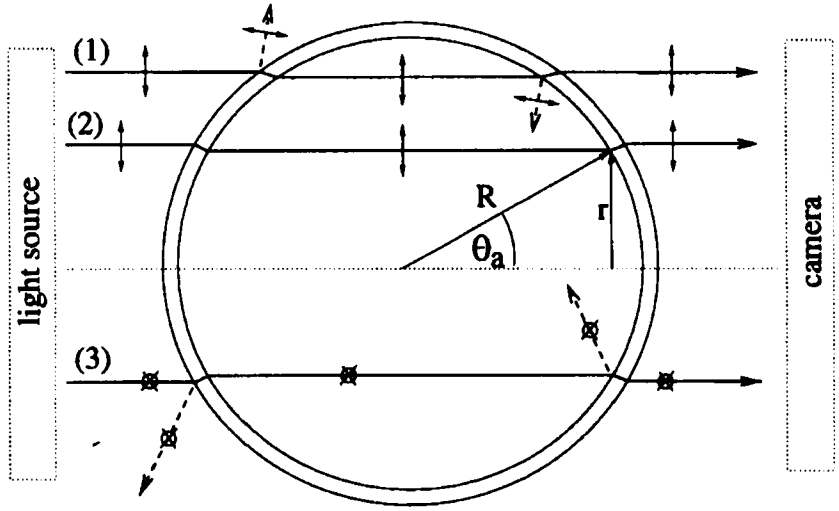

FIGURE 2 Light beams transmitting the bubble: (1) and (2) are polarized in the plane of incidence, (3) perpendicular to that plane; (membrane thickness disproportionally enlarged.)

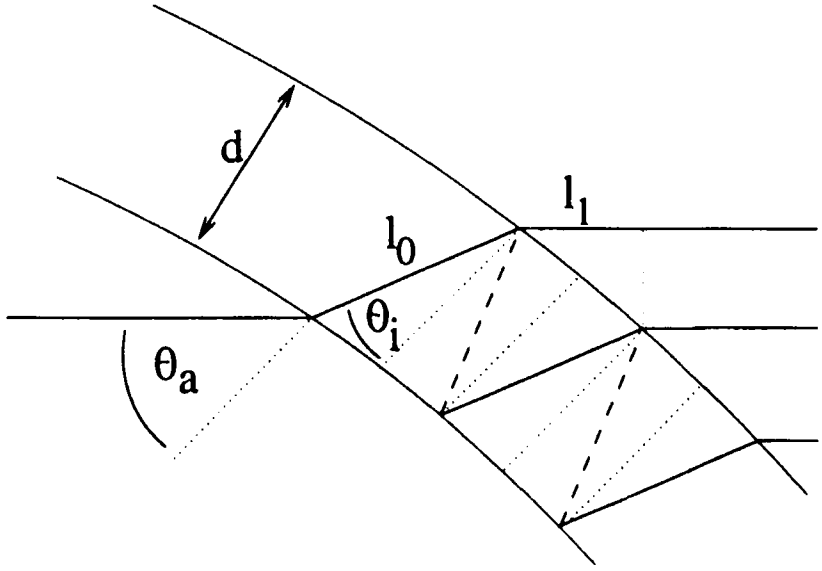

FIGURE 3 Sketch of the transmitted and multiply reflected beams in the bubble membrane. The film curvature is much exaggerated in this scheme

Exiting the film the directly transmitted beam has the phase $\phi_0 = 2\pi n_o l_0/\lambda = 2\pi n_o d/(\lambda \cos\theta_i)$ and the corresponding electric field amplitude is

$$A_{0\perp} = (1 - \rho_\perp^2)\exp(2\pi j n_o d/(\lambda\cos\theta_i)). \tag{4}$$

The $2m$ times internally reflected beam has the phase $\phi_m = (2m+1)\phi_0$ after passing the membrane. We have to correct this phase lag with the phase difference outside the film $\varphi_m = 2m\pi n_o l_1/\lambda = 4m\pi n_o d \sin^2\theta_i/(\lambda\cos\theta_i)$ and obtain

$$A_{m\perp} = A_{0\perp}\rho_\perp^{2m}\exp(4m\pi j n_o d\cos\theta_i/\lambda). \tag{5}$$

The total amplitude is found by summation $A_\perp = A_{0\perp}\Sigma_{m=0}^{\infty}A_{m\perp}$ and the transmitted intensity is

$$I_\perp = A_\perp A_\perp^* = \frac{1}{1 + 4\rho_\perp^2/(1-\rho_\perp^2)^2\sin^2(2\pi n_o d\cos\theta_i/\lambda)}. \tag{6}$$

From Snell's law one obtains $\cos\theta_i(r) = \sqrt{1 - \left(\frac{r}{n_o R}\right)^2}$. In the center of the image ($\cos\theta_i = 1$) the equation is the same as for a planar film at normal incidence with minima $I_\perp = 4n_o^2/(n_o^2+1)^2$ at $d = (2\kappa+1)\lambda/(4n_0)$ and maxima $I_\perp = 1$ at $d = \kappa\lambda/(2n_0)$, $\kappa = \{1,2,..\}$. For thin films ($4n_o d < \lambda$), the transmission intensity $I_\perp(r)$ continuously decreases towards the outer border of the image.

Eqs. (2–6) can be easily adopted to the calculation of $I_\parallel$. Inside the medium, n_o has to be replaced by the effective refractive index $n_1 = \sqrt{n_o^2 + (1 - n_o^2/n_e^2)(r/R)^2}$. Transmission and reflexion coefficients for the amplitudes change to

$$\tau_\parallel^{(in)} = \frac{2\sin\theta_i\cos\theta_a}{\sin(\theta_i+\theta_a)\cos(\theta_i-\theta_a)} \text{ and } \tau_\parallel^{(out)} = \frac{2\cos\theta_i\sin\theta_a}{\sin(\theta_i+\theta_a)\cos(\theta_i-\theta_a)} \text{ resp.}$$

The internal reflection coefficient is $\rho\| = \tan(\theta_a - \theta_i)/\tan(\theta_a + \theta_i)$ and the transmitted intensity is

$$I_\parallel = \frac{1}{1 + 4\rho_\parallel^2/(1-\rho_\parallel^2)^2\sin^2(2\pi n_o d\cos\theta_i/\lambda)}. \tag{7}$$

There exists a position r for any film thickness d where the transmitted intensity $I_\parallel$ is 1 (Brewster angle, beam (2) in Fig. 2).

The bubble membrane is passed twice by the light beam (see Fig. 2), therefore we have to multiply the calculated transmittivities of the rear and front half-spheres, coherences can be neglected. When the thicknesses of rear and front membrane are equal, one obtains $I_\perp{}^2$ and $I_\parallel{}^2$, respectively. The complete transmission intensity $I_n$for unpolarized light is

$$I_n(r) = [I_\parallel{}^2(r) + I_\perp{}^2(r)]/2 \tag{8}$$

EXPERIMENTAL OBSERVATIONS

In general, stationary bubbles reach a final state of perfectly homogeneous film thickness. Fig. 4 shows such a uniform DOBAMBC bubble in S_C^* at 85°C together with the calculated transmission profiles for light of different polarization states. It turns out that n_o has the dominating influence on the simulations while optical anisotropy and orientation of the optical axis are of minor importance. The equations derived for S_A are satisfactory approximations also for S_C and $S_{C'}^*$ bubbles, textures are not observed.

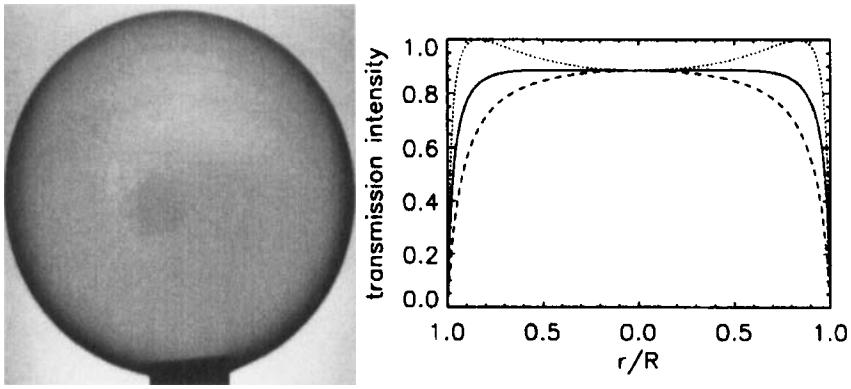

FIGURE 4 Bubble with uniform 70nm membrane in unpolarized λ=589nm light *(left)* and calculated equatorial optical profiles $I_{\parallel}^2$ (dotted), $I_{\perp}^2$ (dashed) and I_n (solid line)

Figure 5 depicts other typical images. The first picture (a) shows a relatively thick but uniform membrane. Non-uniform bubbles can be easily created during the inflation process. Image (b) was taken during rapid inflation of an initially very thick 8CB film. The film thickness continuously decreases towards the top. This state is not persistent. As soon as the inflation stops, an uniform membrane area grows until it finally covers the whole bubble. Image (c) shows a bubble with three regions separated by sharp thickness steps. The borders between these regions shift very slowly, at the timescale of hours. Both the growth of holes at the cost of thick areas and the opposite effect, the climbing of additional layers upwards have been observed in bubbles of stationary radius. In the bubble presented in Fig. 5c, both the top and bottom regions grew and the middle region was extincted, after that the thin top region grew further and finally covered the hole membrane.

An example of hole growth is shown in Fig. 6, two instant images of the same bubble and the time evolution of the hole are presented. Competing effects as

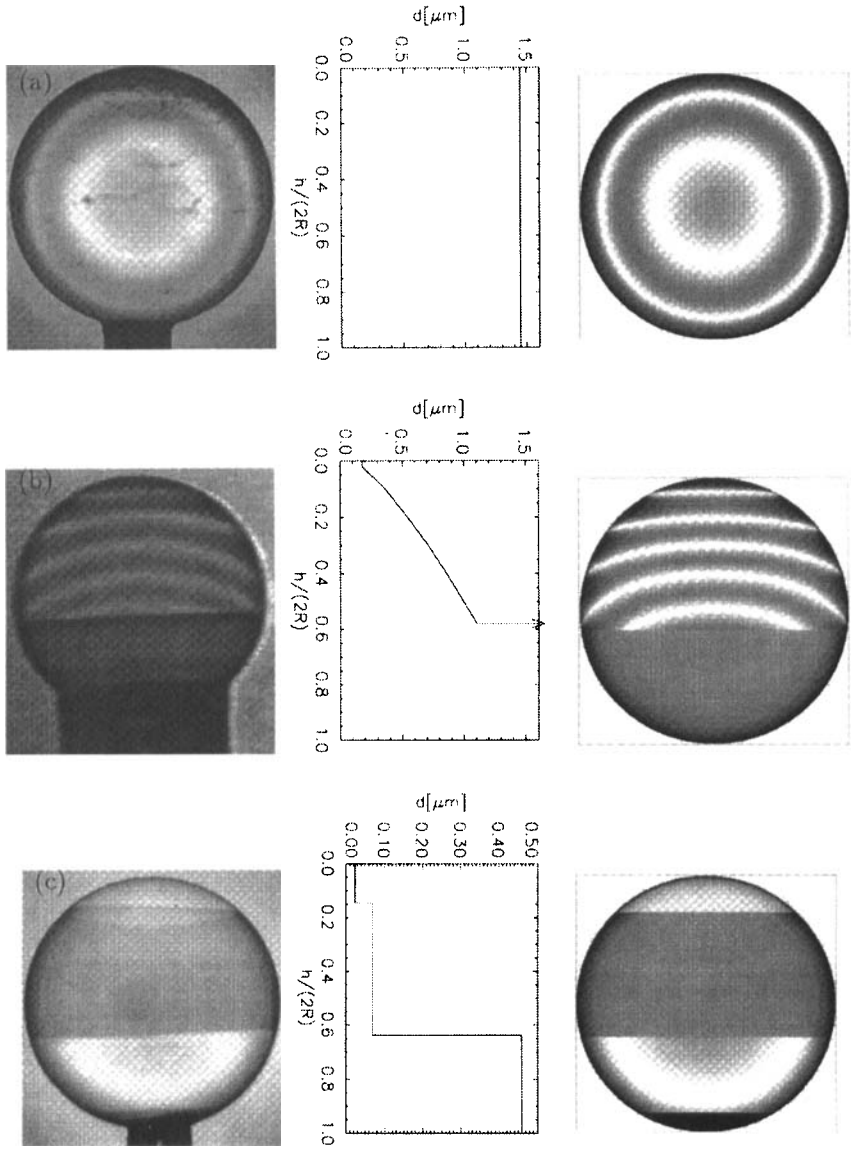

FIGURE 5 Experimental *(left)* vs. simulated *(right)* images and corresponding film thickness $d(h)$ as a function of the vertical coordinate h *(middle)*. **(a)** a very thick homogeneous bubble, circular rings reminding of "Newton" fringes are observed for very thick films ($d > \lambda/n_0$), **(b)** non-stationary state of a bubble with continuously varying film thickness during fast inflation, **(c)** a bubble with two sharp thickness steps

gravity, line tension of the hole boundary and probably even small differences of the surface tension of thin and thick regions influence the hole evolution.

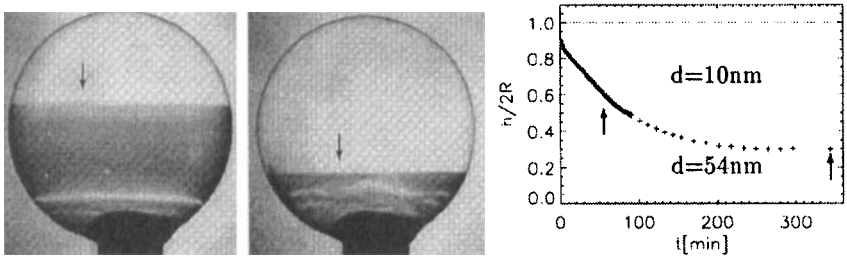

FIGURE 6 Growth of a "hole" in a S_C^* bubble (*Merck* FELIX-16 at room temperature), after ≈1h *(left)*and 6h *(middle)*, The graph *(right)* shows the vertical position of the thickness step vs. time, (h=1 at the top)

The formation of a hole in a homogeneous bubble during inflation is shown in Fig. 7. Unlike the very slow growth dynamics of the hole seen in the previous figure, the motion of the hole on the membrane surface is very rapid, note the different time scales in the graphs (Figs. 6, 7).

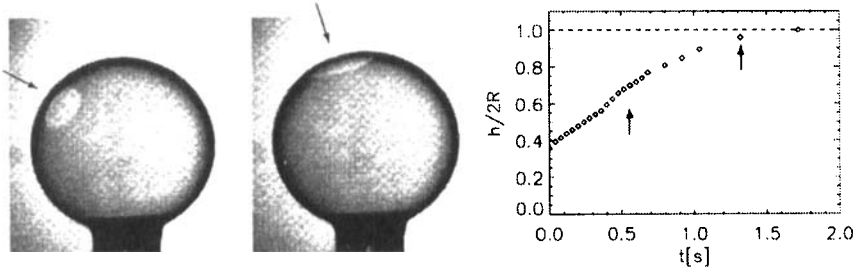

FIGURE 7 Motion of a "hole" (d≈10nm) in a 75nm membrane towards the top, 8CB at room temperature, images after 0.56s *(left)* and 1.32s *(middle)*, contrast much enhanced. The top is reached after ≈ 1.5*s*. The graph shows the vertical position of the center of the hole vs. time

SUMMARY

The optical simulations allow a determination of the film thickness *d*from bubble images in parallel monochromatic light. We have determined the vertical variation of *d*in uniform and non-uniform bubbles. The final state reached in most experiments was a uniform film thickness on the sphere. Bubbles with two or

more sharply separated thickness plateaus are often observed after inflation. These regions are long-term persistent but not stationary. We have found no general trend favouring thinner or thicker regions. Instead, both the climbing of excess layers (hole shrinking) as well as the retraction of excess layers (hole growth) have been observed.

Only during rapid inflation (growth $\approx$ 1 *mm/s*) of thick films, we observe a quasi-continuous spatial film thickness variation as seen in Fig. 5b.

The dynamics of islands on smectic films has been studied only scarcely so far, for example the formation of islands in vibrating films has been described[7,8] and discussed in terms of inertial forces. On the sperical bubble surface we observe a high mobility of holes and islands. The rising of holes to the bubble top is driven by gravity and damped by the in-plane velocity gradients. A qualitative analysis of the hole mobility on bubble surfaces and its relation to viscous properties of the film is in progress.

Acknowledgements

We acknowledge H. Groothues and C. Thieme for contributions to the experiments. This study was supported by the DFG within *SFB 294*.

References

[1] for recent reviews see, e.g. Ch. Bahr; *Int. J. Mod. Phys. B* **8** 3051 (1994). T. Stoebe, C.C. Huang; *Int. J. Mod. Phys. B* **9** 2285 (1995).
[2] P. Oswald *J. Physique* **48** (1987).
[3] R. Stannarius, Ch. Cramer; *Europhys. Lett.*, **42** 43, (1998).
[4] R. Stannarius, Ch. Cramer; *Liq. Cryst.* **23** 371, (1997).
[5] M. Born, *Optik* (Springer, Berlin, 1985).
[6] I. Kraus et al. *Phys. Rev. E* **48** 1916 (1993).
[7] H. Dumoulin, M. Brazovskaja, P. Pieranski; *Europhys. Lett.* **35** 505 (1996).
[8] M. Brazovskaja, H. Dumoulin, P. Pieranski; *Phys.* Rev, *Lett.* **76** 1655 (1996).